PERGAMON

Journal of Atmospheric and Solar-Terrestrial Physics 64 (2002) 915–922

Journal of ATMOSPHERIC AND SOLAR-TERRESTRIAL PHYSICS

www.elsevier.com/locate/jastp

Modulation of upper mesospheric temperature inversions due to tidal-gravity Wave interactions

R.J. Sica[a,*], T. Thayaparan[b], P.S. Argall[a], A.T. Russell[a], W.K. Hocking[a]

[a] *Department of Physics and Astronomy, The University of Western Ontario, London, Ont., Canada N6A 3K7*
[b] *Defence Research Establishment Ottawa, National Defence, Ottawa, Canada*

Abstract

Two nights of coincident measurements with the University of Western Ontario's MF radar and Purple Crow Lidar have been extensively analyzed to illustrate the possible effects due to tidal-gravity wave interactions on upper mesospheric inversion layers. On both nights an inversion layer in the upper mesosphere disappears as the westward component of the tide increases. Inversions similar in height and magnitude to these two nights, as seen in the nightly mean temperature profile, occur in 11% of the measurements made by the Purple Crow Lidar since 1994. Of these inversions, 76% show similar behavior to the two nights considered here in detail. The statistical results suggest the upper mesospheric inversion occur in two types. The first type, illustrated by the individual nights considered in this study, are associated with increased gravity wave variance as the magnitude of the westward tide decreases. These inversions are persistence over many hours. The second type of inversion has a similar nightly mean structure, but is due to shorter (on the order of <2 h) periods of heating with temperature changes much greater than that expected from tidal dissipation.

Keywords: Mesosphere; Temperature; Inversion; Lidar; Gravity waves

1. Introduction

The role of gravity waves in driving the mesospheric thermal structure away from radiative equilibrium, and the filtering of gravity waves by the mean wind, is now well established (Lindzen, 1981). Furthermore, radar measurements have demonstrated that in addition to filtering by the mean wind, gravity wave filtering can occur due to the changing rhythms of the tides (e.g. Fritts and Vincent, 1987).

It is well known that temperature inversions on the order of tens of degrees routinely occur in the mesosphere and lower thermosphere (e.g. Schmidlin, 1975; Hauchecorne et al., 1987). Leblanc and Hauchecorne (1997) have studied the seasonal variations of inversions and found that the inversions are stronger in the winter months at midlatitudes, while during the summer months the strongest inversions occur at lower latitudes. They also found that many inversions had an extended longitudinal structure, as opposed to being local phenomena.

What is the cause of these inversions? Most explanations of mesospheric inversion layers involve atmospheric waves, though Whiteway et al. (1995) have suggested that the inversions form due to turbulent mixing in a manner similar to the formation of the planetary boundary layer. Hauchecorne et al. (1987) suggested that the inversions are due to gravity waves breaking within the inversion region for extended periods. Evidence that tides are also involved was presented by Dao et al. (1995) and States and Gardner (1988). Subsequently, Meriwether et al. (1998) have suggested that tidal modulation of gravity wave forcing is the key to the formation of the inversions. Current reviews of observations (Meriwether and Gardner, 2000) as well as modeling (Liu et al., 2000) discuss these issues, as well as differences in inversions measured above and below the mesopause.

In this study we use measurements of temperature and kinetic energy density from the Purple Crow Lidar (PCL)

* Corresponding author. Fax: +1-519-661-3129.
E-mail address: sica@uwo.ca (R.J. Sica).

1364-6826/02/$ - see front matter
PII: S1364-6826(02)00046-9

Rayleigh-scatter system, in addition to simultaneous tidal determinations by the University of Western Ontario's (UWO's) MF radar, to study upper mesospheric inversion layers. We define an upper mesospheric inversion layer to be a region where there is an inversion with a mean temperature perturbation of 2 K or greater (averaged over at least 5 h) at heights greater than >70 km. We present in detail two nights' coincident measurement which show the inversion layers occurred during times of increased gravity wave energy deposition in the inversion region. These increases in gravity wave energy deposition are shown to be modulated by the zonal component of the wind.

2. Methodology

2.1. Purple crow lidar Rayleigh-scatter measurements

To study the temporal variation of mesospheric inversion layers, a high temporal-spatial resolution measurements of temperature is required. Suitable measurements for these purposes were obtained using the PCL Rayleigh-scatter system. The lidar's transmitter is a frequency-double Nd:YAG laser with a pulse energy of nominally 600 mJ and a pulse repetition rate of 20 Hz. The receiver is a 2.65 m diameter liquid mercury mirror. The lidar is located at The University of Western Ontario's Delaware Observatory (42°52′N, 81°23′W). Details of the apparatus are available in Sica et al. (1995). The temperature analysis employed is based on the scheme described by Chanin and Hauchecorne (1984), which require an initial seed temperature at the top of the measurement region to determine the temperature profile. The choice of temperature is an uncertainty, whose contribution to the total error is not known precisely without an independent knowledge of the true temperature. The contribution of this uncertainty decreases by a factor of 10 approximately every 2 scale heights below the initial height of the integration. If the model atmosphere, (Fleming et al., 1998), seed temperatures are accurate to 10% (e.g. 20 K), then in the upper mesosphere the effect of the seed temperature is on the order 2 K or less for this study, as the integration of the individual profiles began at or above 95 km. Of course, if the seed temperatures are accurate to 1%, the contribution to the total error is only 0.2 K in the inversion region. The choice of seed temperature has no affect on the density perturbations used for the spectral analysis.

Gravity wave energy deposition is found from vertical-wavenumber correlograms (Tsuda et al., 1989) computed using measured density deviations from the mean state as described by Sica and Russell (1999). Though the correlogram analysis suffers resolution limitations relative to parametric modeling techniques, it is robust and is well-suited for determinations of total energy deposition. As described by Sica and Russell (1999) the correlograms were converted into kinetic energy density spectra using the gravity wave polarization relations.

Two nights were selected for analysis. The density perturbation data series were computed for the upper mesosphere, here taken to be 67.5–85 km, from density profiles obtained at 144 m vertical resolution and 4 min temporal resolution. The background state density was estimated using a fifth-order polynomial as described by Gardner et al. (1989). Once the background state is removed, the individual data series are detrended by subtracting their mean, thus avoiding obscuring of the low-frequency spectral regions, as shown by Sica and Russell (1999). Also, detrending the individual data series removes the mean density from each series, but preserves variance associated with differences in the densities from the background state. Thus, density (and hence, temperature) perturbations are independent of overall background-state changes. The density perturbations are then smoothed temporally with a Kaiser–Bessel filter with a bandwidth of 84 min.

Correlograms determined from the density perturbations typically utilized 40 lags. In each case the correlogram was integrated from the low-wavenumber peak of the spatial correlogram out to 1/(3333 m). This choice of high-wavenumber cutoff was limited by the photon noise floor of the spectrum, which is removed from each correlogram. The results are insensitive to this choice of high-wavenumber cutoff, since the majority of the power in the vertical wavenumber spectrum is usually at lower wavenumbers.

2.2. UWO MF radar measurements

The UWO MF radar operates at a frequency of 2.219 MHz and transmits 20 kW of peak power with a duty cycle of 0.12%. The pulse repetition frequency is 60 Hz and a 32-point coherent integration is employed. This data rate gives an effective sampling interval of 0.533 s. The radar has been in operation since November, 1992 and has been used to measure returns via the spaced antenna method in the 49–142 km height range, though only measurements in the 85–94 km range were used to determine winds in this study. Wind measurements are made at time intervals of 5 min and at 3 km height intervals. The configuration for the receivers is three antennas in an equilateral triangle with a spacing of 225 m. The transmitter uses a 3×3 array of dipoles with 150 m spacing. The complex auto-correlation and cross-correlation functions obtained from a 512-point time series are parameterized to obtain true velocity estimates using a full correlation analysis. A more detailed description of the MF radar system is given by Thayaparan et al. (1995a, 1997).

For this study data sets with a bandwidth of 2 days coincident with the PCL measurements were chosen, with the beginning of the epoch at 0000 UT on the day of the lidar measurements. A 2-day fit was used as it is of sufficient length to give reasonable significance to the results, yet short enough to give a reasonable sensitivity during periods of enhanced tidal activity. The raw measurements in the

Table 1
Mean wind and amplitude of the tidal components (m/s) as determined by the MF radar

Measurement period	Mean	24 h	12 h
Zonal			
June 1–2, 1996	2.6	7.0	9.8
July 31–August 1, 1998	4.5	2.5	5.6
Meridional			
June 1–2, 1996	− 12.0	6.0	8.3
July 31–August 1, 1998	− 12.7	10.5	9.6

Table 2
Phase of the tidal components (in local time) as determined by the MF radar

Measurement period	24 h	12 h
Zonal		
June 1–2, 1996	0500	1954
July 31–August 1, 1998	1742	0612
Meridional		
June 1–2, 1996	2318	0530
July 31–August 1, 1998	2000	0418

85–94 km height range at 3 km intervals have been averaged before performing the analysis. Averaging over this height range is a reasonable choice, since the tidal phases are found to be almost constant over the period of observation. Furthermore, the averaging increases the signal-to-noise ratio of the determinations and guarantees a continuous data set. It should be noted that 93–95% of the total available raw wind data were available after the averaging during these periods. Generally, the data were distributed fairly evenly throughout each period, ensuring that there was no bias due to sampling effects.

The 2-day data sets were analyzed for each period of observation using a harmonic analysis technique that includes the mean, 48, 24, 12 and 8 h components (e.g. Thayaparan et al., 1997). The meridional and zonal components of the amplitude and mean wind for the two periods analyzed are given in Table 1, while the phases are given in Table 2. Wind fluctuations variances in 2-h intervals were also computed. We make the usual assumption that these residual oscillations are due to gravity waves. A median filter was then applied to the residuals, so that residuals lying outside of the 95% significance level were rejected in each 2-h interval when estimating the gravity wave variance. The variances are then compared to the tidal components to determine if they are correlated. A more detailed description of the analysis procedure is given by Thayaparan et al. (1995b).

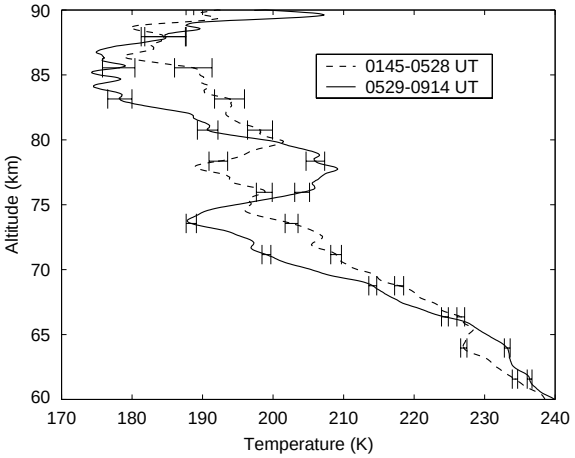

Fig. 1. Average temperature of the mesosphere in the first half of the night's measurements compared to the second half of the night's measurements on July 31, 1998 at 48 m height resolution, smoothed with a 1008 m bandwidth filter. For reference, 0000 UT is 1900 EST. The error bars show the statistical error of the measurement.

2.3. Height overlap of the measurements

As described above, the radar tidal determinations reflect an average at nominally 90 km altitude. The lidar temperature measurements are from 30–90 km altitude. Furthermore, the inversions to be discussed in the following section occur in an altitude range from 75 to 80 km.

3. Individual nights

3.1. July 31, 1998

3.1.1. Temperature

Fig. 1 shows the average temperature of the mesosphere in the first half of the night's measurements compared to the second half of the night's measurements. The measurements have been processed at 48-m height resolution. An upper mesospheric inversion layer is evident in the second half of the night (solid line). Below this region the lapse rate is much steeper than in the first half of the night, where the lapse rate is closer to a typical value expected from empirical temperature models. Fig. 2 shows the changes in temperature as a function of height and time. The mesospheric inversion occurs during the second half of the measurement period, where between 75 and 79 km the average temperature is 15–20 K higher in the second half of the measurement period when compared to the first half. Above and below this region the temperature is 15–20 K cooler during the second half of the measurement period.

3.1.2. Gravity wave total kinetic energy density

The total gravity wave kinetic energy density for the upper mesosphere is shown in Fig. 3. After 0545 UT the upper

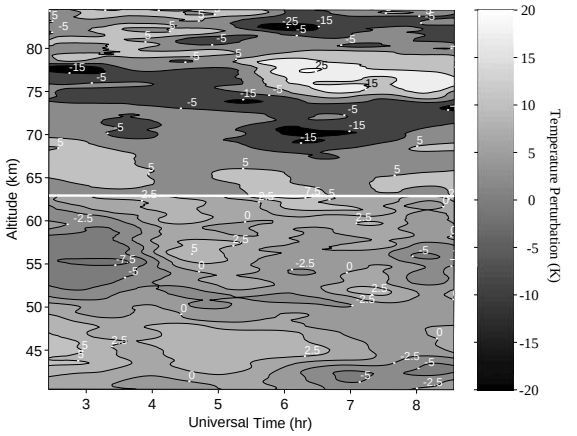

Fig. 2. Temperature perturbations from the mean state on July 31, 1998 at a spatial resolution of 144 m and a temporal resolution of 4 min. The perturbations have been smoothed in space with a 1008 m bandwidth filter and in time by a 84 min bandwidth filter. The contour lines are 2.5 K apart in the lower part of the figure and 10 K apart in the upper part of the figure, since the measurement signal-to-noise ratio is greater at lower altitudes. The contour steps are greater than the maximum statistical errors and thus represent geophysical variations of the temperatures. A color version can be downloaded at http://pcl.physics.uwo.ca.

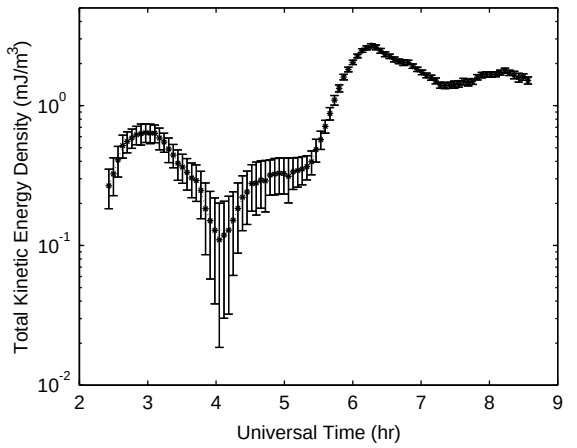

Fig. 3. Total kinetic energy density as determined from the PCL density perturbation measurements on July 31, 1998 in the upper mesosphere (67.5–85 km).

mesospheric kinetic energy densities increase in concert with the temperature in the inversion region.

3.1.3. Upper mesospheric tides

Tables 1 and 2 give the tidal components for a 2-day period beginning at 0000 UT on July 31, 1998. Fig. 4 shows that the semidiurnal tidal component is significantly correlated with the radar-derived RMS gravity wave variance, with an essentially zero lag time (solid line). The diurnal

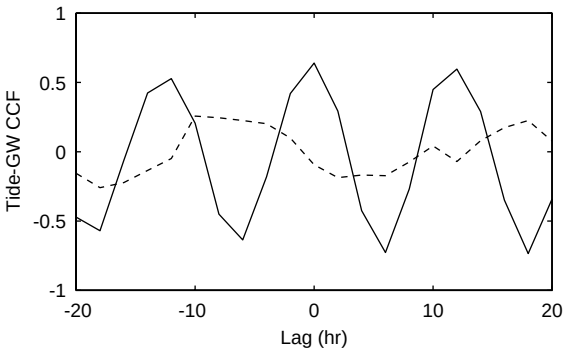

Fig. 4. The cross correlation of the semidiurnal (solid line) and diurnal (dashed line) zonal tide with the residual RMS wind variance determined by the MF radar.

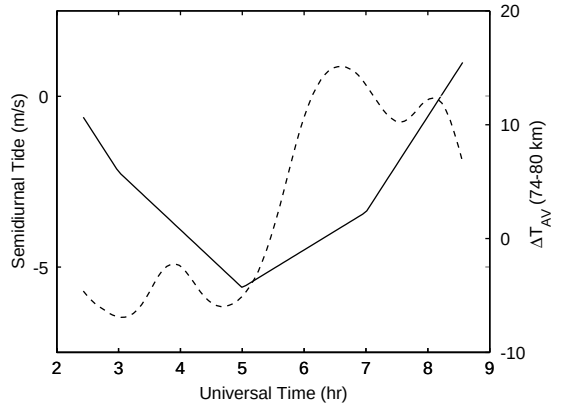

Fig. 5. The semidiurnal tide (solid line, left-hand axis) and the average temperature change between altitudes of 74 and 80 km (dashed line, right-hand axis) on July 31, 1998.

tide exhibits significantly less correlation with the wind variance.

3.1.4. Correlations between temperature and tides

Results from the previous section suggest that during the second half of the lidar measurement period the effects of wave filtering by the mean wind is less than the first half of the night. This result, along with the correlation between the gravity wave variance and the semidiurnal tide, suggests that the temperature change in the inversion region could be correlated with the semidiurnal tide. Fig. 5 shows the semidiurnal tide and the mean temperature change from 74 to 80 km altitude. The cross correlation between the semidiurnal tide and the mean temperature in the inversion region is maximum (-0.8) at a lag of 2 h, which means the temperature increased rapidly with decreasing westward velocity. Including the mean wind, the total of the mean wind plus the semidiurnal tide has a minimum value of about -1 m/s around 0500 UT.

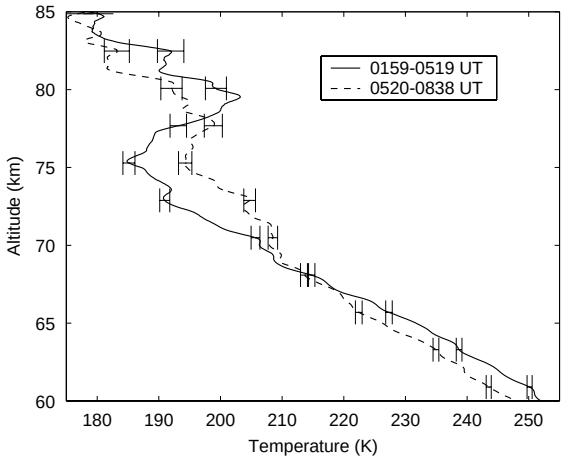

Fig. 6. Average temperature of the mesosphere in the first half of the night's measurements compared to the second half of the night's measurements on June 1, 1996 at 48 m height resolution, smoothed with a 1008 m bandwidth filter. For reference, 0000 UT is 1900 EST. The error bars show the statistical error of the measurement.

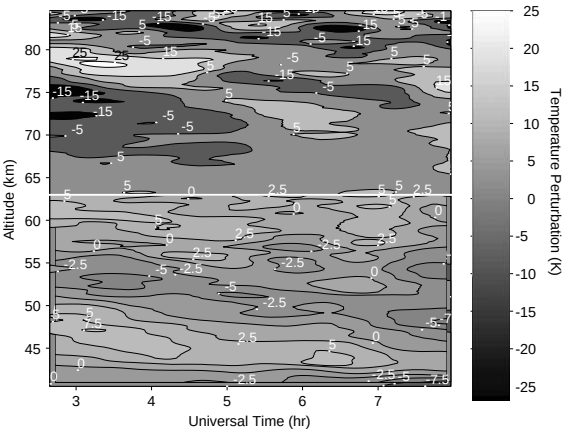

Fig. 7. Temperatures perturbations from the mean state on June 1, 1996, in the same format as Fig. 2. A color version can be downloaded at http://pcl.physics.uwo.ca.

3.2. June 1, 1996

3.2.1. Temperature

The mesospheric temperature profile on June 1, 1996 is similar to July 31, 1998, but in this case the inversion occurs in the first half of the evening (Fig. 6). Fifteen kilometers below the inversion layer, the mesopause has a large average lapse rate, much greater than that expected from empirical models and consistent with July 31, 1998. A comparison of Figs. 2 and 7 shows that the magnitude, temporal extent and height structure in the mesospheric structure is similar

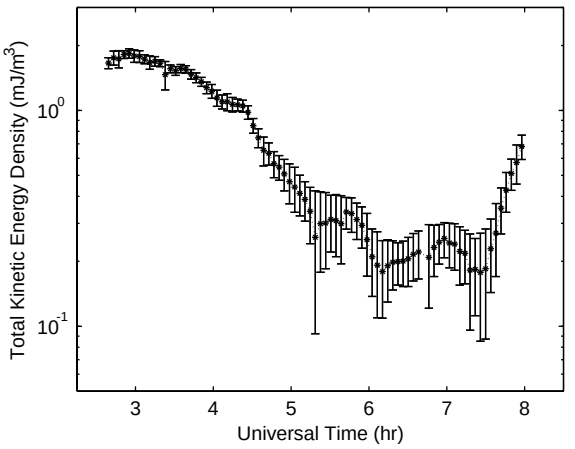

Fig. 8. Total kinetic energy density as determined from the PCL density perturbation measurements on June 1, 1996 in the upper mesosphere (67.5–85 km).

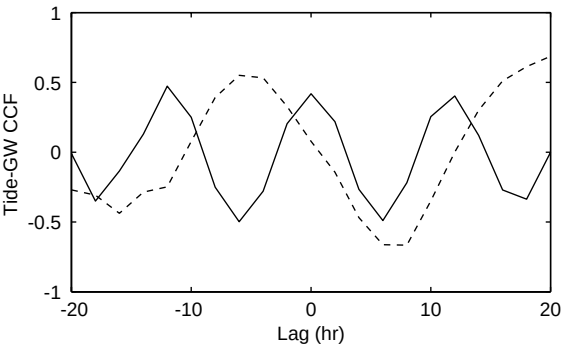

Fig. 9. The cross correlation of the semidiurnal (solid line) and diurnal (dashed line) zonal tides with the residual RMS wind variance determined by the MF radar.

to that of July 31, 1998, except now the inversion occurs in the first half of the observing period.

3.2.2. Gravity wave total kinetic energy density

The upper mesospheric kinetic energy densities are at a maximum when the inversion is strongest, and then decreases by a factor of almost 10 as the inversion weakens (Fig. 8). The magnitude of the kinetic energy densities is similar on this night compared to July 31, 1998.

3.2.3. Upper mesospheric tides

In contrast to the measurements of July 31, 1998, the semidiurnal and diurnal tidal components (Tables 1 and 2) are equally correlated with the radar-derived gravity wave variances, though in this case the correlation coefficient is about 0.5 (Fig. 9).The diurnal tide lags the gravity wave variance by about 5 h, while the semidiurnal component is essentially in phase with the wave variance.

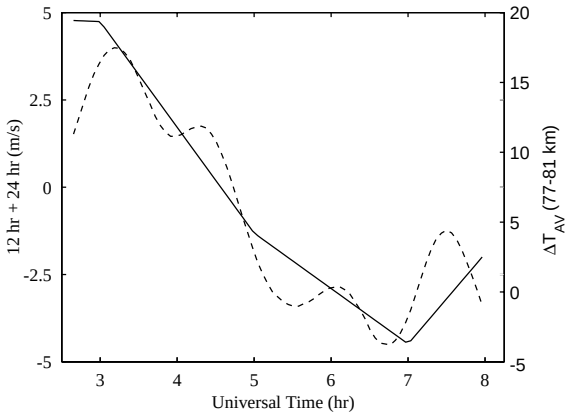

Fig. 10. The sum of the diurnal and semidiurnal tides (solid line, left-hand axis) and the average temperature change between altitudes of 77–81 km (dashed line, right-hand axis) on June 1, 1996.

3.2.4. Correlations between temperature and tides

Unlike the previous case where only the semidiurnal tide was considered, the correlations shown in Fig. 9 suggest that the temperature change in the inversion should be compared to the sum of the diurnal and semidiurnal tides. During the period of lidar measurements the semidiurnal tide is changing strongly from eastward to westward, while the diurnal tide is switching from westward to eastward. Fig. 10 shows the sum of the diurnal and semidiurnal tide compared to the average temperature change between altitudes of 77 and 81 km. The tide changes from eastward to westward, with the zero-crossing around 0430 UT and an approximately 0 mean value. Though the mean wind is small (2.6 m/s; see Table 1) it is large enough to offset the winds to decreasing eastward velocities from 0300 to 0600 UT. The cross correlation between the total tide and the temperature change has a maximum at 0 lag with a reasonably significant (0.6) cross-correlation coefficient. The average temperature changes in the same sense as on July 31, 1998 that is as the wind speed weakens in the eastward direction the strength of the inversion decreases.

4. Statistical context

How representative are the nights chosen for this study? To answer this question a statistical analysis of 308 nights of PCL measurements was undertaken. Of these 308 nights, 223 nights extended over 5 h or more. These 223 nights were searched for mean nightly inversions >2 K at heights above 70 km. The mesopause was identified and care was taken to insure that the inversion search did not occur above the mesopause. Table 3 lists the 25 nights which had inversions satisfying the above criteria. These nights were compared to the nights of July 31, 1998 and June 1, 1996, presented in Section 3. Of these nights, 19 had inversions with durations >10 h (some of these longer duration inversions did not show any modulation effects at all, i.e. they were present over the entire measurement period). The other six nights had more intermittent inversions, that is to say inversions with higher frequency (on the order of an hour or two) changes over the night's measurements. It should be emphasized that all but two of the 19 longer period inversions are in the May–August period. Though the lidar measurements have a sampling bias from May to August, 72 of the 223 nights are in the September–April period.

Table 3
PCL measurement nights with upper mesospheric inversions >2 K. See the text for details

Night	Measurement duration (h)	Possible tidal modulation	Comment
940807	7	Yes	Double inversion, 84 km inversion modulated, 74 km inversion present all night
940816	6	Yes	Inversion present all night
941012	10.5	Yes	Inversion present all night
950703	6	Yes	
960601	6.5	Yes	
960805	7	Yes	Inversion present all night
960807	6	No	
960809	7.25	Yes	Inversion present all night
960811	7	Yes	Inversion present all night (some modulation during <1 h period)
970605	6	Yes	
971218	12	No	
980216	12	Yes	Inversion present all night
980710	6	Yes	
980712	6.5	No	
980713	6.5	No	
980716	5	No	
980718	5	Yes	Inversion present all night
980731	7	Yes	
980813	8	Yes	
990520	6.5	Yes	
990521	6.5	No	
990701	5.5	Yes	Near top of measurement range
990711	7	Yes	Inversion present all night
990712	6.5	Yes	Double inversion, 82 km modulated, 76 km inversion present all night
990716	5.5	Yes	

5. Summary, discussion and future work

Coincident measurements with the University of Western Ontario's MF Radar and Purple Crow Lidar show the dynamic nature of upper mesospheric inversion layers. These measurements suggest a relationship between inversion layers and changes in the kinetic energy density of the gravity wave vertical wavenumber spectrum, as well as modulation of the inversion layers by tidal variations. Though the measurements are coincident in time, the radar tidal determinations are nominally at 90 km altitude, while the inversions observed by the lidar are in the altitude range from 75 to 80 km. If the tidal phase has an appreciable height variation, the relation between changes in these two height regions becomes difficult to interpret. However, detailed comparisons between MF radar measurements and the Global-Scale Wave Model (Hagan et al., 1999) have shown this model to be reliable for determinations of the diurnal and semidiurnal tide in the upper mesosphere. The Global-Scale Wave Model predicts phase variations of the semidiurnal tide at summer solstice in the 70–90 km altitude range to be small (e.g. < 1 h) at these latitudes, meaning a straightforward comparison of the measurements between these two heights is a reasonable expectation (see http://www.hao.ucar.edu/public/research/tiso/gswm/gswm.html to view these and other interesting results from the Global-Scale Wave Model).

While none of these pieces of the inversion puzzle are new, the measurements presented here are perhaps the most compelling that are available which suggest the relation between tides, gravity waves and this class of upper mesospheric inversions. This relation of increasing gravity wave activity during inversions considered here is likely due to changes in the filtering of waves by the tides, changes which allow more wave energy to reach the upper mesosphere and lower thermosphere during periods of enhanced temperatures, a process shown in Fig. 6 of Thayaparan et al. (1995).

The nights of June 1, 1996 and July 31, 1998 exhibited upper mesospheric inversion layers. On July 31 the semidiurnal tide was dominant and highly correlated with the gravity wave variance. As the semidiurnal tide decreased in its westward phase the inversion layer appeared. June 1 is a more complicated example, with the gravity waves being more highly correlated with the sum of the diurnal and semidiurnal components. Again, as the amplitude of the westward phase of the total tide decreased, the strength of the inversion increased.

The combined effect of both the mean and tidal circulations on these nights is such that the overall circulation during these periods is almost entirely eastward during the period of lidar measurements. This eastward bias in the mean wind would allow for considerable growth of westward traveling gravity waves, and, depending on the phase of the tide, slower moving eastward waves. As the total of the mean and tidal wind becomes more strongly eastward then more waves have the opportunity to reach the upper mesosphere, which appears to be the case for the periods when the inversion is present.

The dynamic nature of the upper mesospheric temperature inversions can be masked by long-term averaging (i.e. over a night), or possibly missed entirely by instruments which fail to sample the inversion during an "on" state (such as a spacecraft which sampled only a single local time). Though the inversion layers are dynamic and are always accompanied by extended regions of increased lapse rate below, they do no appear to be associated with significant changes in atmospheric stability (as indicated by lidar-derived lapse rates).

These measurements, as well as other evidence, suggest that (at least) two distinct types of upper mesospheric inversions may occur. The first type, as suggested by the nights presented here, is intimately related to tides. Though the inversion magnitudes are larger than expected from tides, the tides are fundamental to controlling the gravity wave momentum and energy density entering the mesosphere from below. The second type of "inversion" may be due to intense gravity waves breaking events. For a nightly average measure, such as that by a lidar, an inversion at a given height could result from short period heating episodes due to a breaking gravity wave. Of course, the conditions for wave breaking can be set by the tides themselves. These second type of "gravity-wave" inversions are distinct from the more intense lower mesospheric inversions which persist for many tens of hours and are almost always present during winter. Perhaps these events are linked to planetary wave activity as well as tides and gravity waves. Further coincident measurements may help address these important questions.

Acknowledgements

We would like to thank the National Science and Engineering Research Council, the Meteorological Service of Canada and the Centre for Research in Environmental Science and Technology (CRESTech) for their financial support and Mr. C. Bryant for his oratory skills at the AGU.

References

Chanin, M.L., Hauchecorne, A., 1984. Lidar studies of temperature and density using Rayleigh scattering. In: Vincent, R.A. (ed.), Handbook for MAP: Ground-Based Techniques, Vol. 13, Paper 7. Scientific Committee on Solar Terrestrial Physics, International Council of Scientific Unions, Urbana, IL.

Dao, P.D., Farley, R., Tao, X., Gardner, C.S., 1995. Lidar observations of the temperature profile between 25 and 103 km: evidence of strong tidal perturbation. Geophysical Research Letters 20, 2825–2828.

Fleming, E.L., Chandra, S., Schoeberl, M.R., Barnett, J.J., 1988. Monthly mean global climatology of temperature, wind, geopotential height, and pressure for 0–120 km. NASA Technical Memorandum 100697.

Fritts, D.C., Vincent, R.A., 1987. Mesospheric momentum flux studies at Adelaide, Australia: observations and a gravity wave-tidal interaction model. Journal of Atmospheric Science 44, 605–619.

Gardner, C.S., Senft, D.C., Beatty, T.J., Bills, R.E., Hostetler, C.A., 1989. Rayleigh and sodium lidar techniques for measuring middle atmosphere density, temperature, and wind perturbations and their spectra. In: Liu, C.H. (ed.), World Ionosphere/ Thermosphere Study Handbook, Vol. 2, ICSU Scientific Committee on Solar Terrestrial Physics, Urbana, IL (Chapter 6).

Hagan, M.E., Burrage, M.D., Forbes, J.M., Hackney, J., Randel, W.J., Zhang, X., 1999. GSWM-98: results for migrating solar tides. Journal of Geophysical Research 104, 6813–6828.

Hauchecorne, A., Chanin, M.L., Wilson, R., 1987. Mesospheric temperature inversion and gravity wave breaking. Geophysical Research Letters 14, 933–936.

Leblanc, T., Hauchecorne, A., 1997. Recent observations of mesospheric temperature inversions. Journal of Geophysical Research 102, 19,471–19,482.

Lindzen, R.S., 1981. Turbulence and stress due to gravity wave and tidal breakdown. Journal of Geophysical Research 86, 9709–9714.

Liu, H.-L., Hagan, M.E., Roble, R.G., 2000. Local mean state changes due to gravity wave breaking modulated by the diurnal tide. Journal of Geophysical Research 105, 12,381–12,396.

Meriwether, J.W., Gao, X., Wickwar, V.B., Wilkerson, T., Beissner, K., Collins, S., Hagan, M.E., 1998. Observed coupling of the mesosphere inversion layer to the thermal tide structure. Geophysical Research Letters 25, 1479–1482.

Meriwether, J.W., Gardner, C.S., 2000. A review of the mesosphere inversion layer phenomenon. Journal of Geophysical Research 105, 12,405–12,416.

Schmidlin, F.J., 1975. Temperature inversion near 75 km. Geophysical Research Letters 3, 173–176.

Sica, R.J., Sargoytchev, S., Argall, P.S., Borra, E.F., Girard, L., Sparrow, C.T., Flatt, S., 1995. Lidar measurements taken with a large-aperture liquid mirror. 1. Rayleigh-scatter system. Applied Optics 34, 6925–6936.

Sica, R.J., Russell, A.T., 1999. Measurements of the effects of gravity waves in the middle atmosphere using parametric models of density fluctuations. Part I: vertical wavenumber and temporal spectra. Journal of Atmospheric Science 56, 1308–1329.

States, R.J., Gardner, C.S., 1988. Influence of the diurnal tide and thermospheric heat sources on the formation of mesospheric temperature inversion layers. Geophysical Research Letters 25, 1483–1486.

Thayaparan, T., Hocking, W.K., MacDougall, J., 1995a. Middle atmospheric winds and tides over London, Canada (43N, 81W) during 1992–1993. Radio Science 30, 1293–1309.

Thayaparan, T., Hocking, W.K., MacDougall, J., 1995b. Observational evidence of gravity wave-tidal interactions using the UWO 2 MHz radar. Geophysical Research Letters 22, 381–384.

Thayaparan, T., Hocking, W.K., MacDougall, J., 1997. Amplitude, phase and period variations of the quasi 2-day wave in the mesosphere and lower thermosphere over London, Canada (43N, 81W) during the years of 1993 and 1994. Journal of Geophysical Research 102, 9461–9478.

Tsuda, T., Inoue, T., Fritts, D.C., Van Zandt, T.E., Kato, S., Sato, T., Fukao, S., 1989. MST radar observations of a saturated gravity wave spectrum. Journal of Atmospheric Science 46, 2440–2447.

Whiteway, J.A., Carswell, A.I., Ward, W.E., 1995. Mesospheric temperature inversions with overlying nearly adiabatic lapse rate: an indication of a well-mixed turbulent layer. Geophysical Research Letters 22, 1201–1204.